# Global atmospheric forcing data for Arctic ice-ocean modeling

Elizabeth C. Hunke[1] and Marika M. Holland[2]

Received 12 April 2006; accepted 9 August 2006; published 27 March 2007.

[1] We compare three forcing data sets, all variants of National Centers for Environmental Prediction (NCEP) forcing, in global ice-ocean simulations and evaluate them for use in Arctic model studies. The data sets include the standard Arctic Ocean Model Intercomparison Project (AOMIP) protocol, standard NCEP forcing fields, and the data set of Large and Yeager (2004). We explore their performance in Arctic simulations using a global, coupled, sea ice-ocean model, and find that while these forcing data sets have many similarities, the resulting simulations present significant differences, most notably in ice thickness and ocean circulation. This underscores the sensitivity of Arctic sea ice and ocean to slight changes in environmental forcing parameters. This study also highlights the difficulties faced by the model intercomparison community attempting to disentangle simulation differences due to model physics from those caused by small differences in forcing parameters. Assessing the simulation uncertainty due to inaccuracies in the forcing data provides context for the simulation uncertainty associated with model physics.

**Citation:** Hunke, E. C., and M. M. Holland (2007), Global atmospheric forcing data for Arctic ice-ocean modeling, *J. Geophys. Res.*, *112*, C04S14, doi:10.1029/2006JC003640.

## 1. Overview

[2] The Arctic Ocean Model Intercomparison Project (AOMIP) is concerned with examining differences in model solutions and their relationship to model physics. This task is complicated by numerous uncertainties in the model forcing data which are particularly large for the data-sparse Arctic Ocean. Evaluation of simulation uncertainty associated with model physics is contingent on the simulation uncertainty due to errors in the forcing data.

[3] AOMIP's mission becomes even more difficult when comparing regional versus global simulations, where lateral boundary conditions in regional models introduce additional forcing differences. Because global models do not specify or restore ocean properties along open lateral boundaries in the ocean as do regional models, Arctic simulations in global models are more affected by forcing at other latitudes. Merging Arctic-specific data or parameterizations with global data sets can exasperate difficulties in global models by creating spurious gradients across the merged latitudes. For model intercomparison projects such as AOMIP, global data are needed that adequately represent Arctic atmospheric conditions yet are consistent with global modeling needs. Specific goals for a data set that fills these various needs are: (1) to reduce errors in Arctic climate simulations caused by poor forcing data or parameterizations, (2) to eliminate merging of global and Arctic-regional data to the extent possible, (3) to reduce interpolation complexity and effort by providing data on the same grid, (4) to increase data consistency by using the same atmospheric height or level, and (5) to allow higher frequency model forcing (up to 4 times daily). Except for radiation, precipitation and runoff, all data fields proposed here satisfy these goals. These three exceptions are annual, monthly mean climatologies. Runoff is the only field still requiring special treatment by modelers, primarily because it is highly grid dependent.

[4] For each forcing data field, we describe the current AOMIP protocol, problems with AOMIP and other forcing data relevant to the Arctic, and propose an alternative. For Arctic modelers, the changes suggested here primarily involve the higher frequency forcing fields; the proposed monthly climatological data is very similar to the forcing currently prescribed. Global modelers will notice more extensive changes in all fields than will regional modelers. Table 1 summarizes the current forcing set used by AOMIP, highlighting data inconsistencies and other problems discussed in the next section.

[5] Analyzing and comparing all available data sets is beyond the scope of this paper. The goal here is to assess the accuracy of the AOMIP forcing data set and to determine the simulation uncertainty associated with small differences in model forcing. Additionally, we seek to compile a forcing set that mitigates problems in the original AOMIP data without significantly altering that forcing, so that subsequent AOMIP simulations are not drastically different from previous runs. Given these goals, we consider only NCAR/NCEP reanalysis data [*Kalnay et al.*, 1996] (hereafter

[1]Climate, Ocean and Sea Ice Modeling Program, Los Alamos National Laboratory, Los Alamos, New Mexico, USA.
[2]National Center for Atmospheric Research, Boulder, Colorado, USA.


0148-0227/07/2006JC003640

**Table 1.** AOMIP Forcing Summary[a]

| Field | Domain | Height | Source | Contraindications |
|---|---|---|---|---|
| | | *Daily Mean* | | |
| atmospheric pressure | 2.5° global | sea level | NCEP | north pole noise, gradients near Greenland |
| temperature | T62 global | 2 m | NCEP | Arctic summer too warm, coastal Antarctic too cold |
| humidity (specific) | Arctic: RH = 90% | – | – | winter RH over ice is |
| | global: merged | 10 m | NCEP | much greater than 100% |
| wind velocity | [model grid] | surface | computed | SLP errors, low frequency, |
| | global: merged | 10 m | NCEP | global data too weak |
| | | *Monthly Mean* | | |
| precipitation | Arctic: 89 × 89 | surface | S-H[b] | climatology |
| | global: T62 | | GPCP | |
| cloud fraction | 320 × 160 global | total | OMIP | climatology |
| river runoff | 14 Arctic rivers | surface | AWI | climatology |
| | global: merged | | GRDC | |

[a]Most acronyms are defined in the text.
[b]*Serreze and Hurst* [2000].

"NCEP") and modifications thereof for the atmospheric state (temperature, humidity, pressure and winds). However, there are options within this data set, such as the domain resolution and height, exemplified in Table 1. Moreover, biases in this data, described in the next section, cause problems for both Arctic and global models. *Large and Yeager* [2004] (hereafter "LY04") produce a new data set for forcing ice and ocean models which is based on NCEP but remedies some of the biases. In this paper we analyze and compare simulations forced using the AOMIP protocol with NCEP and LY04 forcing data. Table 2 outlines the forcing data combinations used for the runs, and Appendix A describes the model configuration. In the "NC" cases, radiation fields are provided instead of cloud fraction; these cases closely follow the "bulk" forcing of *Large et al.* [1997].

[6] In section 3 we present comparisons between 20-year simulations using AOMIP and modified *Large and Yeager* [2004] data. Other papers in this special section [*Holloway et al.*, 2007; *Zhang and Steele*, 2007] (M. Karcher et al., On the dynamics of Atlantic Water circulation in the Arctic Ocean, submitted to *Journal of Geophysical Research*, 2007, hereinafter referred to as Karcher et al., submitted manuscript, 2007) discuss factors affecting Atlantic Layer circulation patterns in the Arctic, concentrating on differences in physical parameterizations among the models. Here we find significant differences in ocean circulation patterns using identical model configurations but with moderately differing surface forcing.

## 2. Forcing Fields

### 2.1. Atmospheric Pressure and Wind

[7] AOMIP utilizes NCEP reanalysis sea-level pressure (SLP) data, provided by the Climate Diagnostics Center as daily means on a 2.5° global grid. The SLP data is used in the computation of surface shortwave (SW) and longwave (LW) radiation, and the calculation of specific humidity, which is then used for latent heat flux and evaporation calculations. Most importantly, it is used for computing surface winds which are then converted to wind stress through bulk formulas. In particular, the AOMIP surface wind components are computed from the atmospheric pressure $p_a$ as

$$\mathbf{W}_s = \begin{cases} 0.8 \begin{bmatrix} \cos 30^\circ & -\sin 30^\circ \\ \sin 30^\circ & \cos 30^\circ \end{bmatrix} \mathbf{W}_g & \text{if } |\mathbf{W}_g| < 15 \text{ m/s}, \\ 0.7 \begin{bmatrix} \cos 20^\circ & -\sin 20^\circ \\ \sin 20^\circ & \cos 20^\circ \end{bmatrix} \mathbf{W}_g & \text{if } |\mathbf{W}_g| \geq 15 \text{ m/s}, \end{cases} \quad (1)$$

**Table 2.** Forcing Data Used for Sensitivity Runs[a]

| | AOMIP | NC | NCw | LY |
|---|---|---|---|---|
| pressure | NCEP daily | $10^5$ Pa | $10^5$ Pa | $10^5$ Pa |
| temperature | NCEP daily | NCEP 6-hourly | NCEP 6-hourly | NCEP + POLES 6-hourly |
| humidity | Arctic RH = 90% + NCEP, daily | NCEP 6-hourly | NCEP 6-hourly | modified NCEP 6-hourly |
| wind | Arctic geostrophic + NCEP, daily | NCEP 6-hourly | NCEP daily | modified NCEP 6-hourly |
| precipitation | S-H + GPCP | S-H + GPCP | S-H + GPCP | S-H + GPCP + X-A[b] |
| cloud | OMIP | (ISCCP) | (ISCCP) | OMIP |

[a]"NCEP" refers to the standard NCEP data described in Table 1 except for temperature, which is 10 m data in all cases except AOMIP. Precipitation and cloud (or radiation) are monthly fields, as is river runoff, which is identical in all cases (see Table 1). The "modified forcing" case follows LY but with humidity additionally modified so that the in situ relative humidity with respect to ice is never greater than 100%.
[b]*Xie and Arkin* [1996].

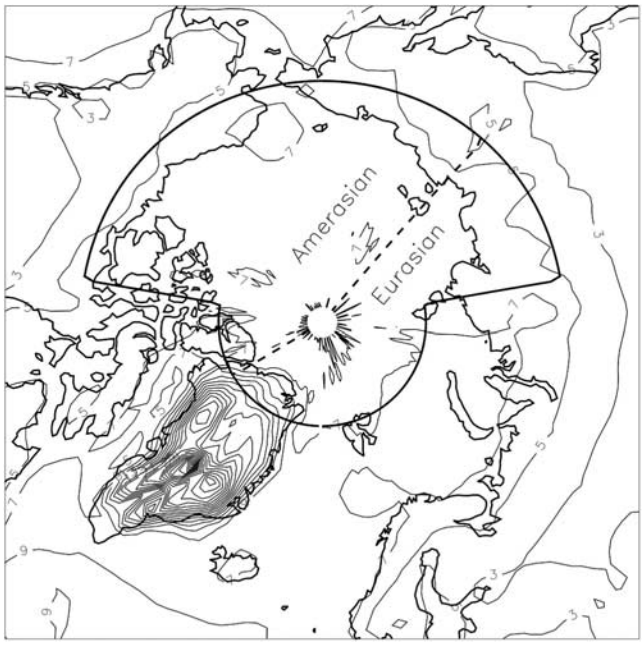


**Figure 1.** Mean annual wind speed for 1982, in m $s^{-1}$. Noise is visible near the north pole, and wind speeds are high along the Greenland coast. Contours range from 1 to 49 m $s^{-1}$, those surrounding the north pole are 7 m $s^{-1}$. In all figures showing "Arctic averages," the averages are taken within the region bounded by the bold curves, omitting land. This region is divided into Amerasian and Eurasian basins by the dashed line, following *Holloway et al.* [2007]. The "hole" at the north pole is a plotting effect.

where

$$\mathbf{k} \times \mathbf{W}_g = -\frac{1}{f\rho_a}\nabla p_a, \tag{2}$$

$f$ is the Coriolis parameter, $\rho_a$ = 1.3 kg $m^{-3}$ is the air density, and **k** represents the vertical unit vector. Surface stress is determined using a wind speed dependent drag coefficient as

$$\tau_a = \rho_a(1.10 + 0.04|\mathbf{W}_s|)|\mathbf{W}_s|\mathbf{W}_s. \tag{3}$$

[8] In the Arctic, NCEP sea level pressure causes two significant problems, illustrated in Figure 1. First is a wave pattern or noise in the vicinity of the north pole. The 2.5° pressure data varies along the row of grid cells whose top edge corresponds to the single geographical point at 90N; this variation gives rise to an apparent wave pattern in the forcing fields computed from sea level pressure and in the ice model output. NCEP air temperature and other fields also exhibit this problem, but other biases in those fields are more significant.

[9] The second problem with the sea level pressure data occurs near Greenland, apparently associated with the high topographic relief [e.g., *Wu et al.*, 2004]. This leads to anomalous fluxes of heat, moisture and momentum in areas of the North Atlantic critical to the global thermohaline circulation and where exchanges between Arctic and Atlantic waters take place.

[10] Additionally, the AOMIP wind derivation is not valid for lower latitudes, so global modelers must merge AOMIP winds with another data source. Moreover, averaging the wind components from 6-hourly to daily alters global surface heat fluxes (discussed later).

[11] *Large and Yeager* [2004] note that NCEP winds are weak compared with scatterometer data. Unfortunately, the scatterometer data only exist for a few years. Thus for their data, LY04 multiply the long record of NCEP winds by a spatially dependent factor that brings the NCEP wind climatology into better agreement with the scatterometer data.

[12] We compare runs with the AOMIP protocol to simulations that use constant sea level pressure, SLP = $10^5$Pa, where needed for radiation and humidity parameterizations and use LY04 10-m wind components. Varying sea level pressure is not critical in the radiation or specific humidity parameterizations, compared with other approximations in those parameterizations as discussed below.

### 2.2. Air Temperature

[13] NCEP air temperatures are too warm in summer months, resulting in excessive sea ice surface melting. Buoy measurements described by *Rigor et al.* [2000] indicate that air temperatures over ocean areas with sea ice remain near the freezing point in summer months. These observations are incorporated into the POLES data set (Polar Exchange at the Sea Surface [*Zhang et al.*, 1998]), which LY04 used to correct NCEP temperatures in the Arctic. Figure 2 shows air temperature from various data sets averaged over the Arctic

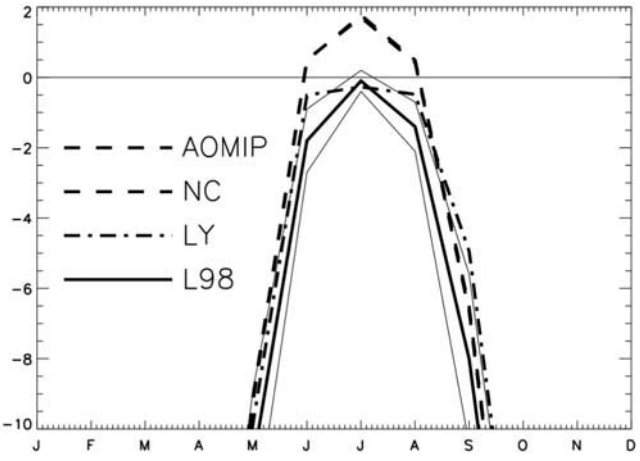


**Figure 2.** Summer 1982 air temperatures, averaged over the Arctic, from AOMIP and NCEP (2 m, identical), LY04 (10 m) and *Lindsay* [1998] estimates from Russian drifting ice stations with standard deviations (2 m). "NC" and "LY" are labels for our NCEP- and LY04-based experiments, which use data from other sources for some fields, as described in this section and shown in Table 2.

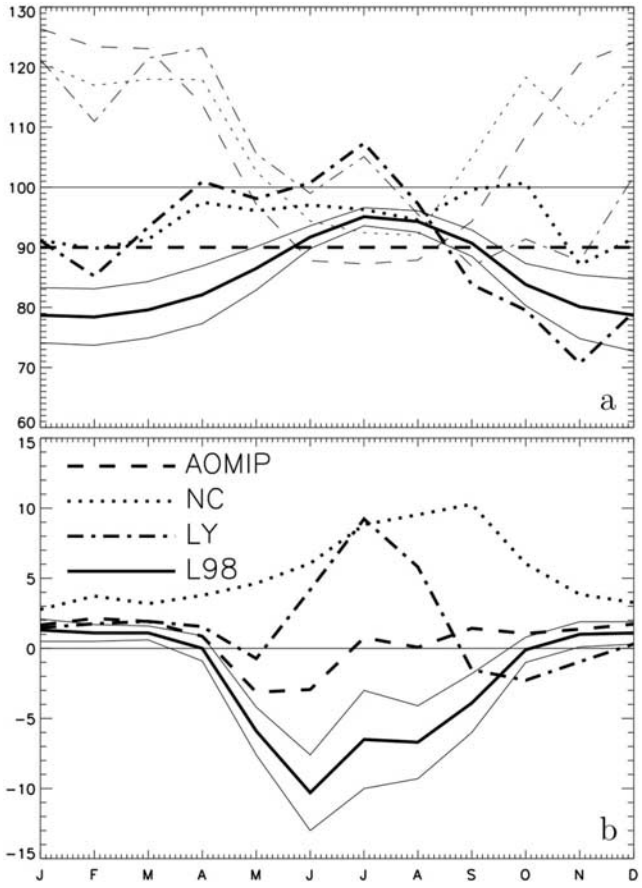


**Figure 3.** (a) Relative humidity (%) and (b) latent heat fluxes (W $m^{-2}$) for 1982, averaged over the Arctic as in Figure 2. Thick lines in (a) indicate relative humidity with respect to water; thin lines show relative humidity over an ice surface (except solid thin lines, which represent one standard deviation in the *Lindsay* [1998] data). Relative humidity is computed following appendix 4 in *Gill* [1982]; latent heat fluxes are into the ice surface (positive downward).

(north of 66N between 100W and 100E, including 0E, and north of 80N for the remaining longitudes, as shown in Figure 1). The AOMIP and NCEP data are identical, with average 2-m temperatures over this large region 0.5–2°C above freezing June through August. The *Lindsay* [1998] data incorporates measurements from Russian drifting ice stations over several decades, and thus is neither spatially nor temporally comparable with the other temperature data shown in Figure 2. Nevertheless, it illustrates the general result that NCEP reanalysis air temperatures are too warm over the summer Arctic. The corrections by LY04 result in cooler Arctic air temperatures March through August, but warmer temperatures for the remainder of the year.

[14] NCEP air temperatures are too cold in the vicinity of Antarctica, especially in winter, possibly due to the high elevations of coastal meteorology stations and the solid sea ice cover used in the NCEP data assimilation model. LY04 correct this bias using a sinusoidal function south of 60S. This correction will not affect regional Arctic simulations.

### 2.3. Humidity

[15] AOMIP specifies a constant relative humidity (RH) of 90% for the entire Arctic, following the procedure employed for the POLES model forcing data set [*Zhang et al.*, 1998]. In POLES, the 90% relative humidity value is combined with POLES air temperature observational data to obtain the specific humidity "data" provided on the POLES web site (http://psc.apl.washington.edu/POLES/model_forcings/ModelForcings.html, J. Zhang, personal communication).

[16] Figure 3a shows that the constant, 90% relative humidity (over water) used by AOMIP compares reasonably well with the *Lindsay* [1998] observational data. However, *Andreas et al.* [2002] have shown from Surface Heat Budget of the Arctic (SHEBA) and Ice Station Weddell measurements that the relative humidity with respect to ice stays near 100% year-round, dropping slightly during the warmer months. They propose a physical mechanism for supersaturation in winter (that evaporation from leads proceeds more quickly than sublimation onto the ice surface is able to remove moisture from the air), but their data do not show ice relative humidities greater than about 105%. The AOMIP protocol data are inconsistent with those observations, as seen in Figure 3a. Ice relative humidities are frequently greater than 110%, with the Arctic-average AOMIP data reaching as high as 125%.

[17] The LY04 data in the Arctic suffer an additional problem because of the temperature correction shown in Figure 2; by reducing air temperature, the correction effectively raises the in situ relative humidity at high latitudes. They reduce the relative humidity by 3% (more at lower latitudes), independently of their air temperature correction in the Arctic, but this reduction does not compensate for the change in relative humidity due to the temperature correction. Thus, even their relative humidity with respect to liquid water becomes supersaturated in the Arctic in July, on average across the entire Arctic Ocean.

[18] This error has the potential to significantly affect surface fluxes over the ice. Whether the atmosphere is supersaturated with respect to the surface determines the sign of the latent heat flux, which in turn helps determine the ice surface temperature and subsequent fluxes. Figure 3b shows Arctic average latent heat fluxes over the ice. Other differences in the data sets besides humidity come into play here: radiation is responsible for the large differences between the NC and LY latent heat fluxes, discussed in section 2.5. Both of these cases show latent heat fluxes of the wrong sign, however, compared with *Lindsay* [1998] fluxes. In cold months, all of the latent heat fluxes are positive, indicating sublimation of water vapor onto the ice surface. In summer negative latent heat fluxes in *Lindsay* [1998] indicate that the ice surface evaporates; positive fluxes in the NC and LY runs mean that the humidity of the air is too large compared with the saturated surface humidity.

[19] We compare simulations using the AOMIP protocol to model runs that use the LY04 10-m humidity fields, which are corrected in an appropriate manner at lower latitudes for global models, but limit humidity at high latitudes such that the in situ relative humidity (i.e., computed with 10-m air temperature rather than surface temperature) with respect to

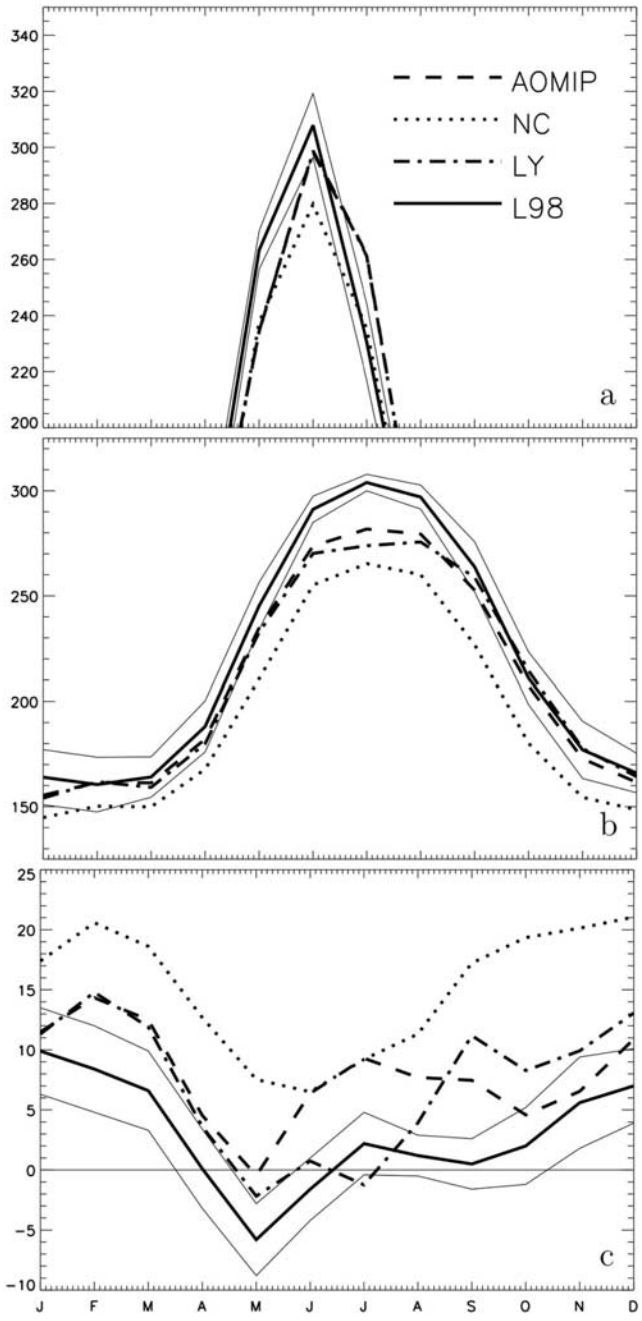


**Figure 4.** (a) Shortwave, (b) longwave and (c) sensible heat fluxes over ice for 1982, averaged over the Arctic as in Figure 2, in W $m^{-2}$. Only summer values in (a) are shown in order to magnify differences in the data during these months.

ice does not exceed 100%. This provides better agreement with relative humidity observations.

[20] This limiting is accomplished, following *Gill* [1982], as follows. Compute the saturation vapor pressure $e_i$ over a planar ice surface from

$$\log_{10} e_i(T) = \frac{0.7859 + 0.03477T}{1 + 0.00412T} + 0.00422T,$$

where $T$ is air temperature in °C. Specific humidity at saturation is then

$$Q_i = \frac{0.622 e_i}{p_a - 0.378 e_i},$$

and the LY04 specific humidity data is limited such that $Q_a \leq Q_i$. For our tests, the limiting is applied globally; this change makes little difference where temperatures are warm. Alternatively, ice area fraction could be incorporated to limit relative humidity only over ice, thus restricting the changes to polar regions and potentially allowing supersaturation as observed in winter. We expect such an ice fraction effect on relative humidity to exhibit less impact on the simulations than the more stringent limiting experiments shown here.

### 2.4. Precipitation

[21] AOMIP currently uses an updated version of the *Serreze and Hurst* [2000] precipitation data set, which covers only the Arctic and is a monthly climatology. Global modelers must merge that data with global precipitation data. For the AOMIP run, we use Global Precipitation Climatology Project (GPCP) combined precipitation data, which were developed and computed by the NASA/Goddard Space Flight Center's Laboratory for Atmospheres as a

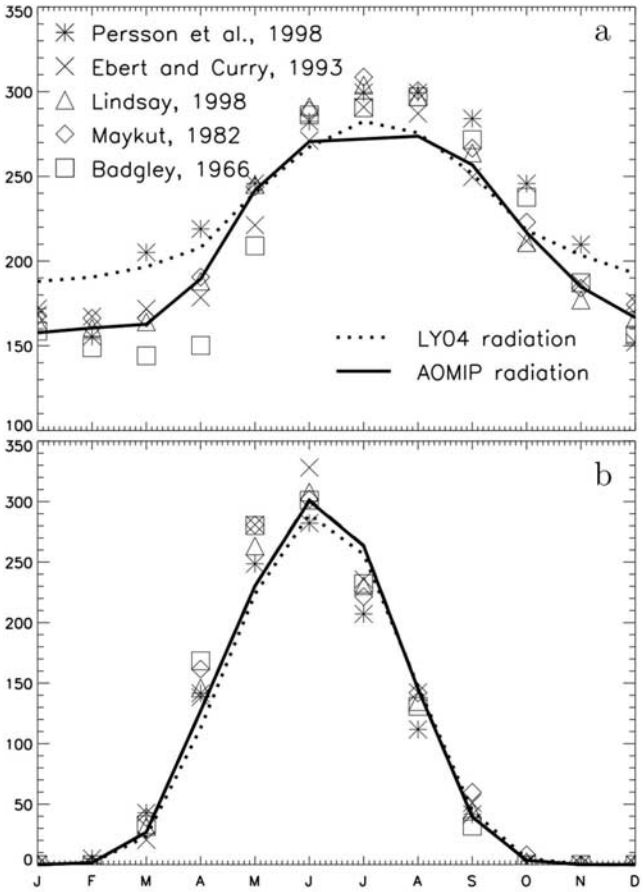


**Figure 5.** Downwelling (a) longwave and (b) shortwave radiation (W $m^{-2}$), averaged over the Arctic for 1981–2000.

**Table 3.** Proposed Forcing

| Field | Domain | Height | Source |
|---|---|---|---|
| | *Six-Hourly Mean* | | |
| pressure | specified constant | | |
| temperature | T62 global | 10 m | LY04 |
| specific humidity | T62 global | 10 m | modified LY04 |
| wind velocity | T62 global | 10 m | LY04 |
| | *Monthly Mean* | | |
| precipitation | T62 global | surface | LY04 normal year |
| cloud fraction | 320 × 160 global | total | OMIP |
| river runoff | | as in Table 1 | |

contribution to the GEWEX Global Precipitation Climatology Project. After studying the available data sets, LY04 merged precipitation data from several sources into one data set suitable for global modeling. In particular, they use GPCP precipitation data south of 60S and 25S–25N, Xie-Arkin data for 65S–30S and 30N–65N [*Xie and Arkin*, 1996], and Serreze and Hurst north of 70N, with 5° blending bands between them. Although LY04 provide yearly fields from 1958, all of them prior to 1979 are simply the climatology. The LY04 "normal year" precipitation fields are the same for the Arctic as in the original AOMIP forcing data; using the LY04 climatology standardizes the data for global modelers and those whose domains extend significantly south of 60N.

### 2.5. Cloud Fraction

[22] Given a cloud climatology, AOMIP modelers currently compute both shortwave and longwave radiation following *Zillman* [1972], *Parkinson and Washington* [1979] and *Rosati and Miyakoda* [1988]. In other data sets such as LY04, downwelling radiation is provided and the cloud fraction used to develop those fields is implicit. The radiation fields also depend on other aspects of the atmospheric state, such as humidity and temperature. The surface state (in particular, whether it is ice-covered or not) is a major factor in all of these data; therefore ice-ocean modelers prefer not to have the surface state from another data set hardwired into the forcing data for their model, preconditioning their results toward the implicit, hardwired ice state. This is particularly important for the radiation data, which are the largest terms in the surface balance. Rather than reading data for shortwave and longwave radiation, AOMIP uses version 2 of the Ocean Model Intercomparison Project's cloud climatology (OMIP [*Röske*, 2001]) along with the temperature and humidity data described above to compute these fields.

[23] Figures 4a and 4b illustrate differences in the radiation formulations. International Satellite Cloud Climatology Project radiation data (ISCCP [*Rossow and Schiffer*, 1991]) used in the NC simulation is much smaller over the Arctic than estimates of *Lindsay* [1998]; AOMIP forcing falls in between. For the LY simulation, radiation is computed as in the AOMIP simulation rather than using the radiation fields available with the Large and Yeager data set; longwave results are slightly different due to setting atmospheric pressure to a constant value and to corrections in the temperature and humidity data described above. Interestingly, the AOMIP formula underestimates shortwave radiation (compared with *Lindsay* [1998]) in May and June, and overestimates it in August and September, potentially introducing a time lag in the Arctic seasonal cycle of ice growth and melt.

[24] LY04 radiation fields, which are based on a newer ISCCP data set, minimize potential surface effects such as those described above (W. G. Large, personal communication). Twenty-year averages (1981–2000) of the LY04 and original AOMIP radiation are shown in Figure 5, along with observed values (LY04 radiation includes interannual variations beginning in 1983). The LY04 forcing data overestimate downward longwave in winter months by 30 W $m^{-2}$. Both data sets underestimate downwelling longwave in summer months. A test simulation using the daily LY04 radiation data results in Arctic ice and ocean fields similar to those in the LY run, but with turbulent fluxes of opposite sign to the *Lindsay* [1998] data and greater ice extent year-round (not shown). Because of these drawbacks, we did not further investigate the LY04 radiation data.

[25] Radiation effects show up most clearly in the sensible heat fluxes over ice, shown in Figure 4c. Here, the AOMIP and LY simulations, which both compute shortwave radiation in the same way but using slightly different data as described above, track the *Lindsay* [1998] estimates well. NC sensible heat fluxes, on the other hand, are always positive and too large. A sensitivity run (not shown) using NC forcing for everything except the radiation fields confirms that this difference in sensible heat flux is primarily due to the radiation forcing. A reduction in downwelling radiation, as between the AOMIP and NC fluxes in Figures 4a and 4b, causes ice surface temperatures to be lower in the NC case, which in turn reduces upwelling longwave radiation. However, the reduction in outgoing radiation only partially compensates for the reduction in downwelling radiation, and except for sensible and latent heat, the other fluxes (such as the conductive flux) affecting the surface heat budget are constrained. As a result, the NC sensible and latent heat fluxes are larger in the positive (downward) direction, making up for the deficit in downwelling radiative fluxes. In a fully coupled simulation with an active atmosphere model, the atmospheric temperature would respond to the cooler ice temperatures, reducing the temperature gradient and thus also the sensible and latent heat fluxes.

### 2.6. River Runoff

[26] Beyond a tabulation of flow rates for major rivers, runoff data becomes highly grid dependent. AOMIP specifies the total runoff in the Arctic using a climatology from the Alfred Wegener Institute (AWI); global modelers merge data from the Global Runoff Data Centre (D-56002 Koblenz, Germany) with that. Each modeler must develop runoff forcing data in a format suitable for use with the individual model grid (coastlines differ, for example); for this reason it is not feasible for AOMIP to provide a runoff data set in a "map" form similar to the other forcing fields. All model runs examined here use identical river runoff forcing as specified in the AOMIP protocol.

### 2.7. Summary

[27] Based on this discussion, we have compiled in Table 3 an improved forcing data set that reduces known biases in the original AOMIP data and provides a more consistent data set for global or regional model simulations

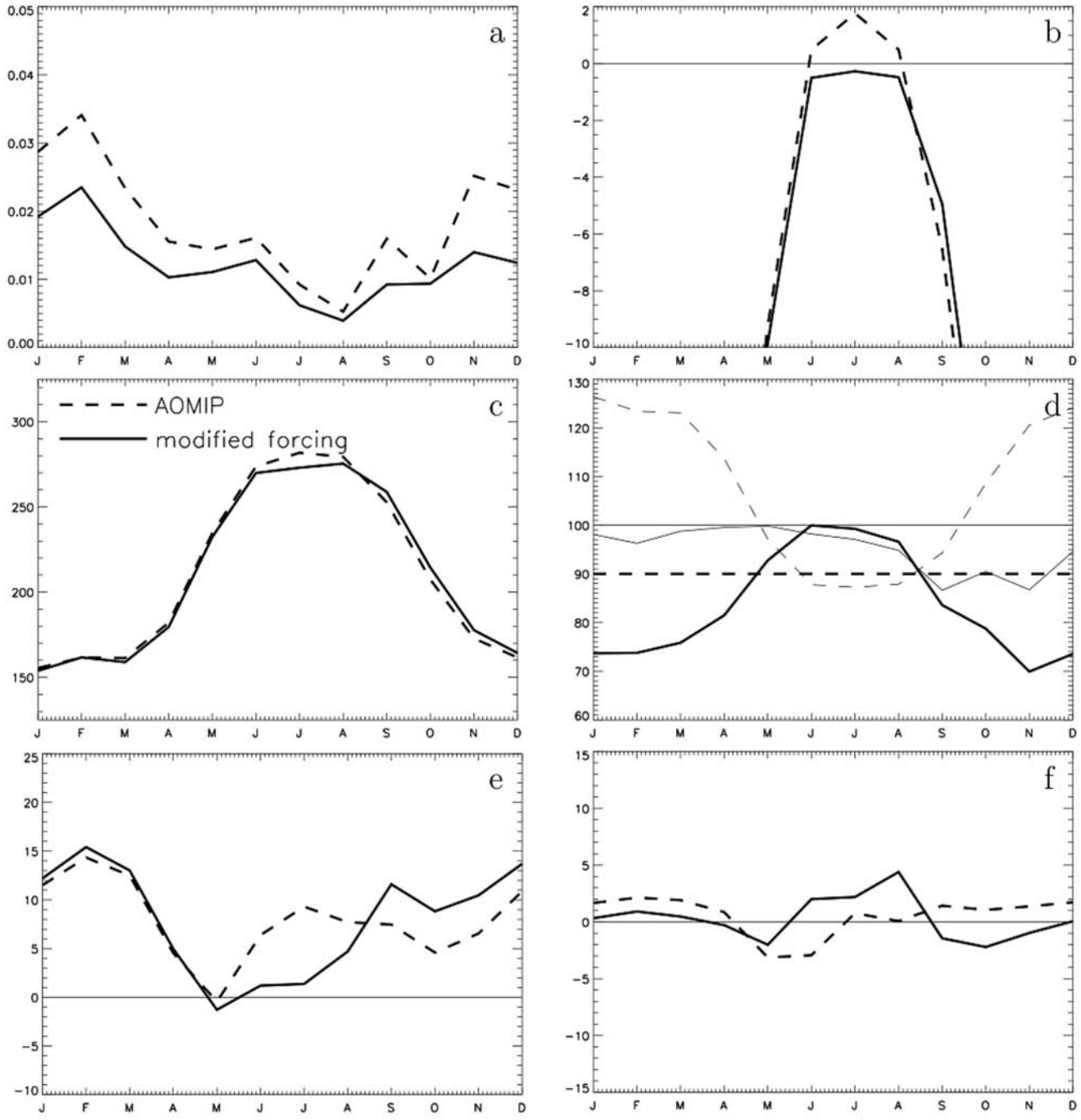


**Figure 6.** (a) Wind stress (N $m^{-2}$), (b) temperature (°C), (c) longwave radiation (W $m^{-2}$), (d) relative humidity (%), (e) sensible heat flux (W $m^{-2}$) and (f) latent heat flux (W $m^{-2}$) for 1982, averaged over the Arctic, for the original AOMIP forcing data and the proposed data set. Thin lines in (d) are relative humidity with respect to ice, and fluxes are positive downward.

that are designed to examine Arctic Ocean processes. The atmospheric state data (temperature, humidity, wind) would all be at 10 m height and available four times daily; almost all of the forcing data would be available on a T62 grid. Monthly mean data is quite similar to that already used by AOMIP modelers.

[28] Biases in temperature and humidity in high-latitude regions are improved over the original AOMIP forcing data; problems with atmospheric pressure data are eliminated by using a constant, approximate value for surface pressure. In spite of changes to the pressure, temperature and humidity, the computed downwelling shortwave radiation is nearly identical to the original over the Arctic (not shown). Figures 6a–6d show Arctic averages of selected forcing fields from the original and modified data sets. Wind speeds are lower in the proposed data, leading to reductions of up to a factor of 2 in the (quadratic) wind stress. Air temperature is lower through August then larger

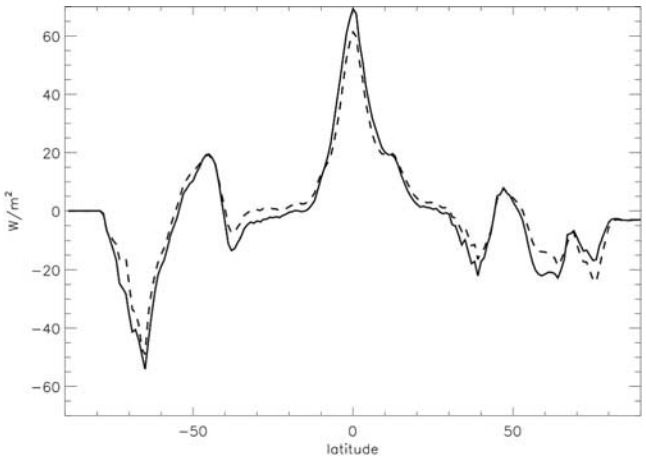


**Figure 7.** Ocean net surface heat flux, averaged into 1° latitude bands for the full 20-year simulations, in W $m^{-2}$, from the 1° runs: (dashed) AOMIP, (solid) modified forcing. Positive values are directed downward.

afterwards, a pattern also reflected in the longwave radiation. Because the radiative fluxes are so similar, the new sensible heat flux (Figure 6e) is also similar to the original AOMIP case, though exhibiting decreases of up to 10 W $m^{-2}$ in the summer months.

[29] The average latent heat flux (Figure 6f) is positive in summer, in contrast to the *Lindsay* [1998] estimates. Our proposed changes to the humidity result in relative humidities that are supersaturated with respect to neither ice nor water, on average, a substantial improvement in the winter months, although the summer months are still too humid. Observations suggest that the relative humidity over ice drops to values around 90% in summer [*Andreas et al.*, 2002], similar to that used in the original AOMIP simulation, whereas in the modified forcing, we only limit the ice relative humidity to 100%. Although the empirical formulas used to convert between relative and specific humidity [*Gill*, 1982] are complex, the relative humidity over ice could be limited by a sinusoidal function that reaches 100% in January, dropping to 90% in July, that might improve the latent heat flux calculation. Such a seasonally dependent parameterization is problematic for global modelers, however.

## 3. Twenty-Year Comparisons

[30] Analyses in section 2, which used the data shown in Table 2 to force a global coupled ice-ocean model on a 0.4° grid, utilized only one year of forcing data (1982) due to the computational expense of running numerous sensitivity studies in this model configuration. To assess the uncertainty in the simulations associated with relatively modest changes in forcing data over a longer time period, we reduced the model configuration to a 1° grid and ran simulations with the original AOMIP forcing and with the forcing data proposed in Table 3 and section 2 for 1981–2000. The simulation using the proposed forcing data is referred to here as the "modified forcing" run. All simulations are performed with the global ocean-ice coupled model as described in Appendix A, on a 1° grid.

[31] Globally, the proposed forcing set yields greater surface heat fluxes into the tropical ocean than the original AOMIP forcing data, but the ocean is cooler elsewhere, as illustrated in Figure 7. Net surface heat flux in the original AOMIP simulation (dashed) is greater than in the modified forcing simulation nearly everywhere. Shorter simulations on the 0.4° grid using the NC forcing, not shown here, exhibited even more ocean cooling than the corresponding

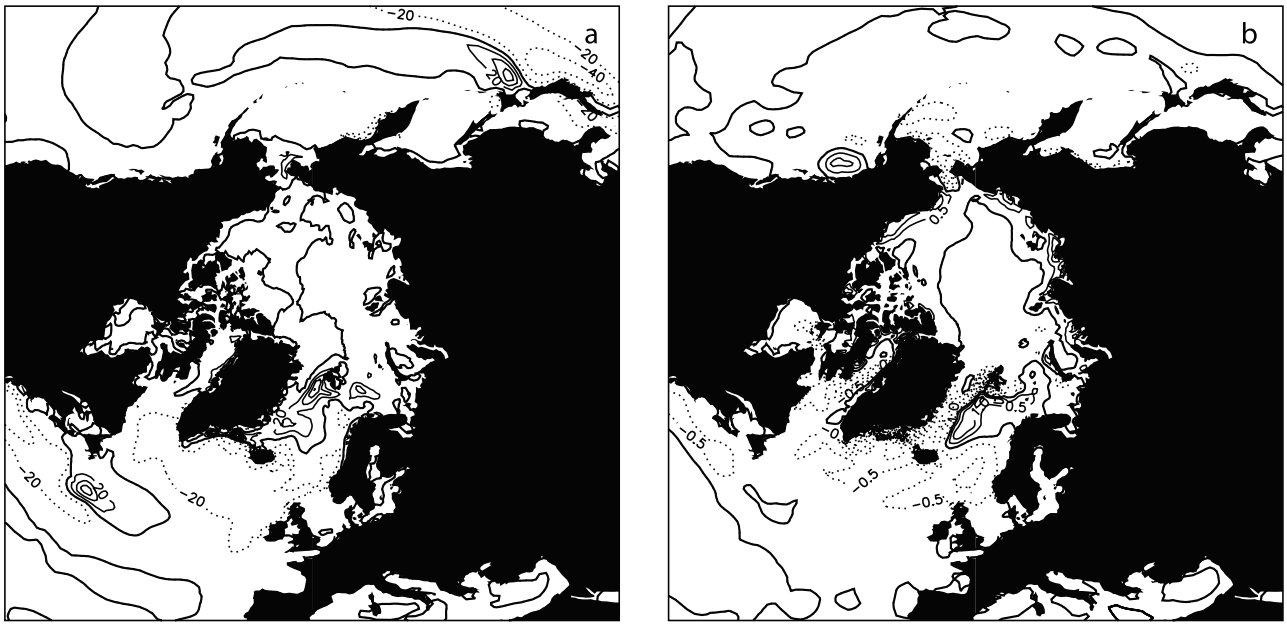


**Figure 8.** Differences in ocean surface (a) heat flux and (b) fresh water flux, averaged for 1981–2000, in W $m^{-2}$, from the 1° runs. Differences are taken as modified minus original, and positive fluxes are directed downward.

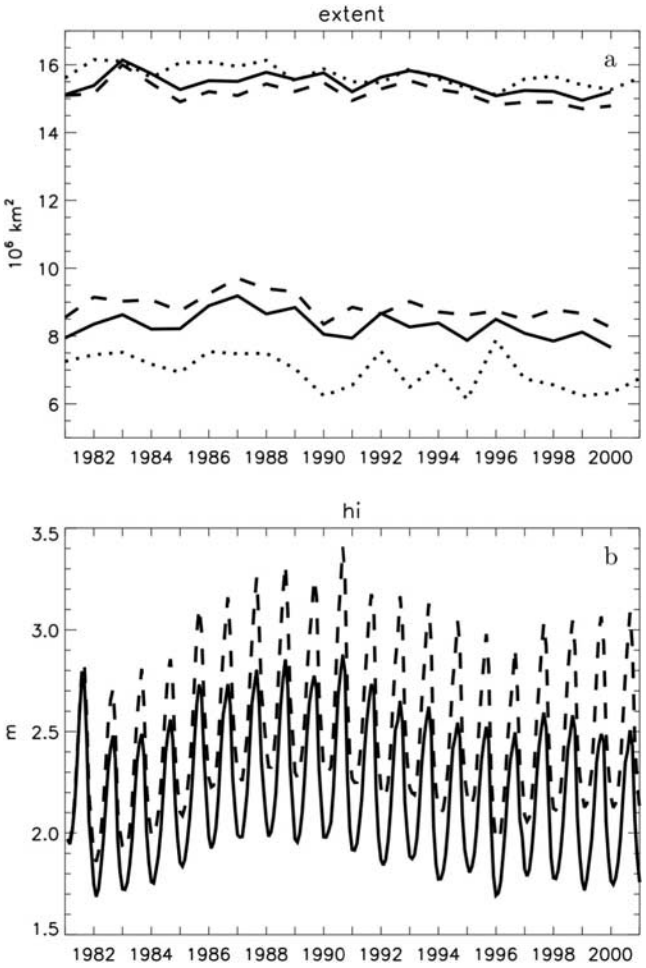


**Figure 9.** (a) Maximum and minimum monthly average sea ice extent and (b) average ice thickness for the AOMIP (dashed) and modified forcing (solid) simulations, for the Northern Hemisphere, from the 1° runs. Dotted lines in (a) show September and March ice extent from satellite passive microwave data [*Fetterer and Knowles*, 2002].

modified forcing run, while averaging the wind components from 6-hourly to once daily (preserving speed) reduced ocean surface cooling slightly, especially in the Antarctic Circumpolar Current (ACC) and western boundary currents.

[32] Figure 8 maps differences in ocean surface heat flux and freshwater flux, averaged over the 20-year simulations. The surface ocean under the modified forcing is cooling more in the North Atlantic than that with the original data, although it is warming in some areas, notably near the ice edge in the GIN Seas and in the Arctic. This difference is reflected in greater fresh water fluxes to the ocean in the modified run along the periphery of the ice pack. The simulated sea ice extent also reflects these differences, shown in Figure 9a. While the maximum winter ice extent is slightly larger in the modified forcing run, the summer ice melts back farther than in the original AOMIP configuration, resulting in a larger seasonal cycle.

[33] The hemisphere-average sea ice thickness is 0.5 m thinner in the modified forcing run (Figure 9), in spite of greater warming in the original AOMIP ocean, illustrated in Figure 10a. Higher wind speeds in the AOMIP simulation lead to a more active ice pack that exhibits greater ridging, open water formation, and subsequent new ice freezing in leads (not shown) which in turn lead to a greater volume of ice over time. Cooler temperatures in the original AOMIP data during the freezing season also contribute to a thicker ice pack.

[34] The Arctic Ocean is warming in both cases, and despite indications given by the sea ice thicknesses, it is warming more in the AOMIP run (Figure 10a). The pattern of warming also differs: the warm Atlantic Layer is deeper in the modified forcing run than in the AOMIP run, while the AOMIP run is much warmer above 500 m (Figure 10b).

[35] The greatest differences between these two simulations appear in the circulation structure, particularly in the western (“Amerasian”) basin. Figure 11 shows the currents at 466 m (model level 19), averaged over the final year of the simulation, 2000. Remarkably, the currents north of Alaska and Canada are flowing in opposite directions. In the modified forcing run, the currents are clockwise, or anticyclonic, and in the AOMIP run they are cyclonic, with a fairly well-defined boundary current in the western Arctic.

[36] These differences in the currents are not limited to just this ocean level nor to just the year 2000. Topostrophy

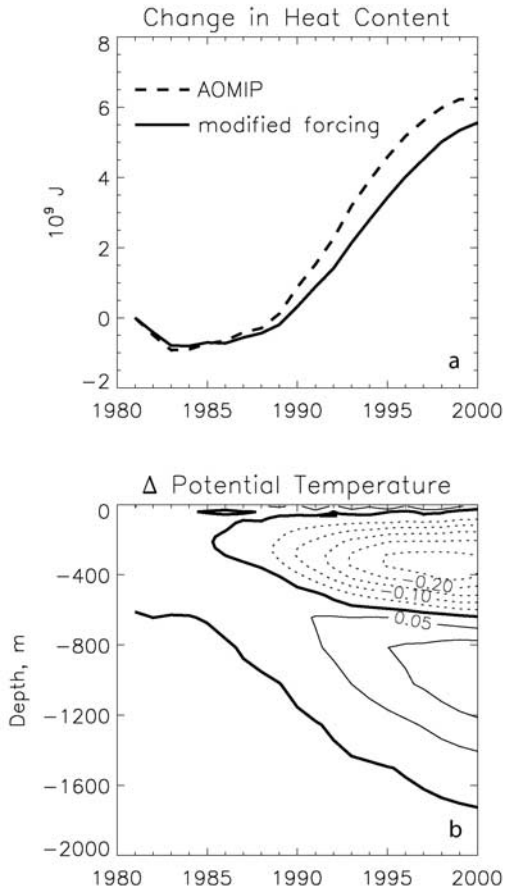


**Figure 10.** (a) Change in total heat content and (b) potential temperature difference (modified minus original) for the modified forcing and original AOMIP simulations, averaged over the Arctic region shown in Figure 1.

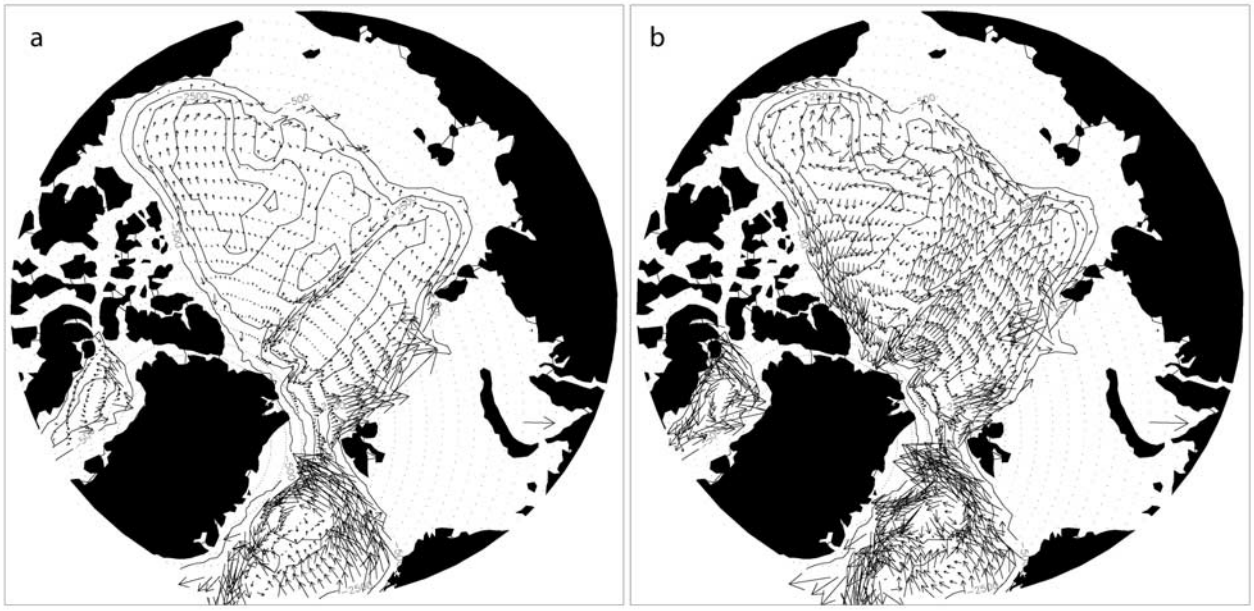


**Figure 11.** Ocean currents at 466 m in the (a) modified forcing and (b) AOMIP simulations, for 2000. The reference vector in the Kara Sea is 1 cm/s. Bathymetry contours are shown every 1000 m, beginning with 500 m.

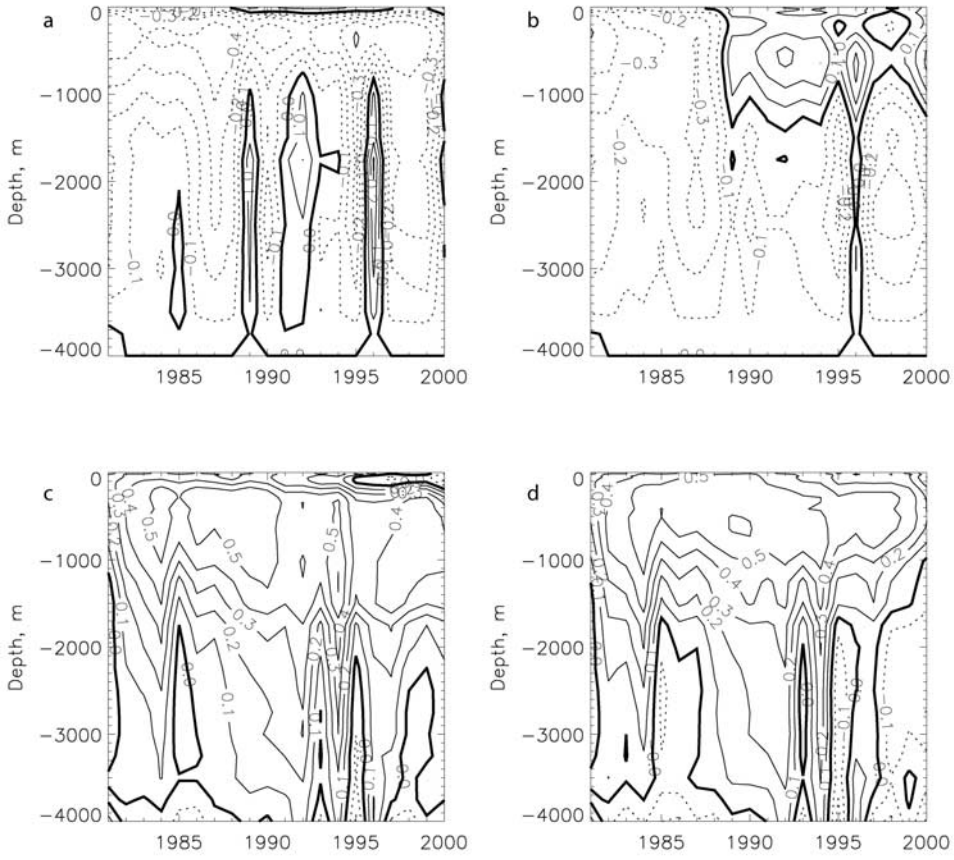


**Figure 12.** Topostrophy for the (left) modified forcing and (right) AOMIP simulations, averaged over (a, b) the Amerasian and (c, d) Eurasian basins, from the 1° runs.

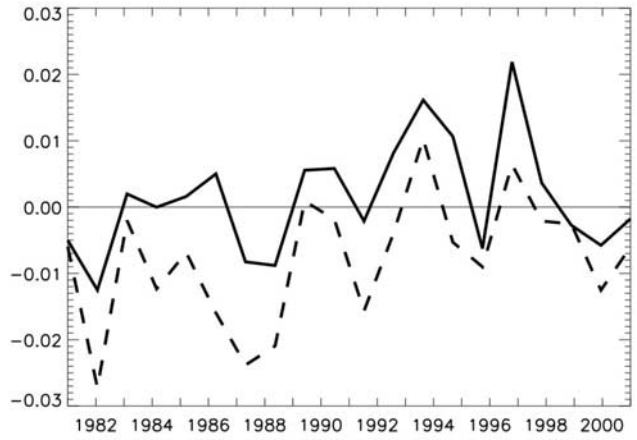


**Figure 13.** Wind vertical vorticity for the (solid) modified forcing and (dashed) AOMIP simulations, averaged over the Amerasian basin. Positive values are cyclonic.

(introduced by *Holloway et al.* [2007]) provides a concise diagnostic for the mean ocean circulation, shown in Figure 12. Here, we see that most of the upper 1000 m of the Amerasian basin remains anticyclonic throughout the modified forcing simulation (Figure 12a), while the simulation using the original AOMIP data becomes cyclonic by 1989 (Figure 12b).

[37] The most significant difference in the forcing data between these two simulations is the wind data. They have similar patterns but the AOMIP wind forcing is considerably stronger than in the modified data set, seen in Figure 6a. Moreover, the winds over this portion of the Arctic tend to be anticyclonic, as illustrated in Figure 13. In fact, winds in the modified forcing data set tend to be more cyclonic than the original AOMIP winds, leading us to conclude that the essential differences in circulation patterns in the upper 1000 m of our simulations are not wind-driven.

[38] Karcher et al. (submitted manuscript, 2007) have investigated the effect of potential vorticity fluxes through Fram Strait and the Barents Sea on ocean circulation in the Arctic. They find that potential vorticity fluxes initially affect the eastern portions of the Arctic, eventually working their way into the Amerasian basin. The circulation shown in Figure 11b appears to confirm this behavior in the present simulations, in spite of basin-averaged topostrophy indicating anticyclonic flow in both simulations (Figures 12c and 12d). A detailed analysis and diagnosis of causes for the circulation differences here are beyond the scope of this paper, but we anticipate that potential vorticity fluxes may play a significant role.

## 4. Concluding Remarks

[39] We have investigated the effects of altering elements of the forcing data used for AOMIP simulations with the goals of reducing known biases and making the data more consistent, especially for global modeling efforts. Of the higher frequency data (daily or six-hourly), we propose adopting the data sets of *Large and Yeager* [2004] for air temperature, humidity and winds, with minor modifications. This results in cooler Arctic summer temperatures, atmospheric humidities that are less humid in winter and moister in summer, and less vigorous wind stresses. These changes result in more realistic model forcing data, as compared with Russian drifting station observations described by *Lindsay* [1998]. AOMIP's monthly Arctic forcing, including radiation, precipitation and river runoff, are relatively unchanged for the tests shown here.

[40] Even with relatively minor changes to the forcing data, we find potentially significant differences in model simulations. Local atmospheric forcing, such as wind and air temperature, is most likely responsible for greater Northern Hemisphere ice volume in the AOMIP run. However, major changes in the ocean circulation patterns are most likely due to differences at lower latitudes that are imported into the Arctic (Karcher et al., submitted manuscript, 2007), highlighting complications that arise when comparing model simulations with different regional domains and differing lateral boundary conditions. It also underscores the considerable simulation uncertainty that is associated with modest changes in environmental forcing conditions.

[41] This document does not address simulation uncertainty or biases associated with numerous other parameterizations, such as the albedo specification. Another parameterization that may considerably affect the simulation behavior is the derivation of wind stress. The AOMIP formula currently specifies a wind speed dependent transfer coefficient, unlike the constant coefficient commonly used in bulk formulas. Other options would be more complicated, such as using stability-dependent transfer coefficients, thereby linking the wind stress and turbulent flux calculations.

## Appendix A: Model Configuration

[42] The LANL AOMIP simulation was performed with an ocean-sea ice coupled model developed at Los Alamos National Laboratory. Detailed documentation for the ocean and ice models can be found in *Smith and Gent* [2002], *Hunke and Lipscomb* [2004] and other publications referenced below. The models are configured following the Arctic Ocean Model Intercomparison Project (AOMIP) protocol and integrated using AOMIP-defined forcing fields and parameterizations, except where noted.

[43] The Parallel Ocean Program (POP [*Smith et al.*, 1992; *Dukowicz et al.*, 1993, 1994]), is a member of the Bryan-Cox class of z-coordinate ocean models that solves the primitive equations for temperature, salinity and the horizontal velocity components. It features an implicit free surface, the UNESCO equation of state formulation of *Jackett and McDougall* [1995], and two-band shortwave penetration with Jerlov water type IB [*Paulson and Simpson*, 1977]. The K-profile parameterization (KPP) provides vertical mixing of momentum and tracers, with convection occurring through a high vertical diffusion coefficient (10 $m^2\ s^{-1}$), done implicitly in time. Lateral mixing of tracers occurs via the GM mixing parameterization [*Gent and McWilliams*, 1990] with $\kappa = 2400\ m^2\ s^{-1}$. Horizontal friction is biharmonic with a coefficient of $-10^{12} \times \cos^3 \phi\ m^4\ s^{-1}$, where $\phi$ is latitude. A third order upwind scheme is used for horizontal advection of tracers while centered differences are used for momentum; bottom

drag is quadratic with a coefficient of $1.225 \times 10^{-3}$. The salinity-dependent freezing temperature is given by $T_f = 0.0575S$, where $S$ is the sea surface salinity, but $T_f$ is limited not to exceed the maximum freezing temperature at the ice bottom (−0.184°C). The ocean model provides sea surface temperature, salinity, currents, slope and a freezing or melting potential to the ice model. The freezing potential is converted to ''frazil ice'' in the ice model; some or all of the melting potential is used to warm and melt the ice.

[44] The Los Alamos Sea Ice Model (CICE) features the energy conserving thermodynamics model of *Bitz and Lipscomb* [1999] with four layers of ice and one layer of snow in each of five ice thickness categories [*Lipscomb*, 2001], the energy-based ridging scheme of *Thorndike et al.* [1975] and *Hibler* [1980], an ice strength parameterization given by *Rothrock* [1975], elastic-viscous-plastic ice dynamics [*Hunke and Dukowicz*, 1997, 2002] and horizontal advection via an incremental remapping scheme [*Lipscomb and Hunke*, 2004]. Prognostic variables for each thickness category include ice area fraction, ice volume, ice energy in each vertical layer, snow volume and energy, and surface temperature. The vertical salinity profile is a nonlinear function of depth with a maximum value at the bottom of the ice of 3.2 psu. Temperature dependence of the longwave radiation and sensible and latent heat fluxes is included in the nonlinear flux balance that (iteratively) determines the ice or snow surface temperature. Surface fluxes and temperatures are computed separately for each ice thickness category and merged based on the fractional area covered by that category. All precipitation over sea ice falls as snow in the model, regardless of the air temperature, and the new snow arrives at the same temperature as the existing snowpack. Snow and ice albedos were never agreed upon by the AOMIP participants; the values used here (0.81, 0.77, 0.70, 0.68 for cold snow, melting snow, cold bare ice, and melting bare ice respectively) are used by two other AOMIP modeling groups and are nearly identical to those used by *Köberle and Gerdes* [2003]. CICE has only one parameter for emissivity (0.98), leading to the other exception to the AOMIP parameters (0.97 for ice and 0.99 for snow). The ice model provides fresh water flux, net heat flux and ice-ocean stress to the ocean model.

[45] When coupled, the ice and ocean models are treated as subroutines, linked through a driver that also reads atmospheric data from files and prepares the data for use by the other components. The driver merges ice and ocean quantities based on the ice area fraction in cells where there is less than 100% ice coverage. The ocean model provides heat for melting the ice based on a turbulent heat flux parameterization whenever the temperature is above the freezing point; new ice formation maintains the ocean temperature at or above the freezing temperature. Virtual salinity fluxes based on the fresh water mass exchange between the ice and ocean contribute to buoyancy forcing at the ocean surface, with a reference ice salinity of 4 psu. Momentum exchange is accomplished through a quadratic ice-ocean drag term computed by the ice model using level 1 (5 m) currents. Turbulent fluxes over ice are computed using bulk formulas following *Parkinson and Washington* [1979]. Over ocean, the formulations of *Kauffman and Large* [2002] are used.

[46] The ice and ocean models are discretized for non-uniform, general curvilinear grids in which the north pole has been moved smoothly into a nearby land mass to avoid prohibitively small time steps or filtering associated with converging meridions [*Smith et al.*, 1995]. For the 0.4° experiments described here, we use a 900 × 600 global mesh (resulting in longitudinal spacing), whose north pole is in North America. The horizontal grid is mercator in the southern hemisphere with latitudinal spacing of $0.4°\cos\phi$. In the northern hemisphere the grid size also decreases with latitude, resulting in a grid spacing that ranges from 9 km (at high latitudes) to 44 km (at the equator). The vertical grid consists of 40 levels which vary in thickness from 10 m at the surface to 250 m at the bottom. Topography was created by merging the Arctic data from *Jakobsson et al.* [2000], *Smith and Sandwell* [1997] data from 72S to 72N, and Southern Ocean data from *Lythe and Vaughan* [2001], followed by pointwise modifications of important sills and channels that may have been smoothed by interpolation to the grid. Where necessary, atmospheric forcing data sets are merged across 60–68N for the AOMIP run.

[47] The driver and ice model use a time step of 30 minutes, while the ocean model time step is slightly longer. The ice model exchanges information with the driver once each time step, the ocean model once per day. The 0.4° sensitivity runs described here are all initialized from the end of year 34 of the AOMIP simulation, which began in 1948 following a 5-year spin-up. Additional details regarding the AOMIP protocol can be found at http://efdl.cims.nyu.edu/project_aomip/experiments/coordinated_analysis.

[48] The 20-year simulations are run on a 320 × 384 (1°) global grid whose north pole is in Greenland [*Kiehl and Gent*, 2004], using a one-hour time step. The spin-up procedure for the ice initial condition followed the AOMIP protocol, but without surface salinity restoring.

[49] **Acknowledgments.** This work was supported by the Climate Change Prediction Program of the Department of Energy's Office of Biological and Environmental Research. We especially thank John Drake and the Center for Computational Sciences at Oak Ridge National Laboratory for extensive use of their Cray X1. Conversations with Mathew Maltrud, William Lipscomb, William Large and other members of the CCSM Polar Climate Working Group were also quite helpful. The National Center for Atmospheric Research is sponsored by the National Science Foundation.

## References

Andreas, E. L., P. S. Guest, P. O. G. Persson, C. W. Fairall, T. W. Horst, R. E. Moritz, and S. R. Semmer (2002), Near-surface water vapor over polar sea ice is always near ice saturation, *J. Geophys. Res.*, *107*(C10), 8033, doi:10.1029/2000JC000411.

Badgley, F. I. (1966), Heat budget at the surface of the Arctic Ocean, in *Proceedings of the Symposium on the Arctic Heat Budget and Atmospheric Circulation*, pp. 267–277, Rand Corp., Lake Arrowhead, Calif.

Bitz, C. M., and W. H. Lipscomb (1999), An energy-conserving thermodynamic sea ice model for climate study, *J. Geophys. Res.*, *104*, 15,669–15,677.

Dukowicz, J. K., R. D. Smith, and R. C. Malone (1993), A reformulation and implementation of the Bryan-Cox-Semtner ocean model on the connection machine, *J. Atmos. Oceanic Technol.*, *10*, 195–208.

Dukowicz, J. K., R. D. Smith, and R. C. Malone (1994), Implicit free-surface method for the Bryan-Cox-Semtner ocean model, *J. Geophys. Res.*, *99*, 7991–8014.

Ebert, E. E., and J. A. Curry (1993), An intermediate one-dimensional thermodynamic sea-ice model for investigating ice-atmosphere interactions, *J. Geophys. Res.*, *98*, 10,085–10,109.

Fetterer, F., and K. Knowles (2002), Sea ice index, http://nsidc.org/data/g02135.html, Natl. Snow and Ice Data Cent., Boulder, Colo.

Gent, P. R., and J. C. McWilliams (1990), Isopycnal mixing in ocean circulation models, *J. Phys. Oceanogr.*, *20*, 150–155.
Gill, A. E. (1982), *Atmosphere-Ocean Dynamics*, 615 pp., Elsevier, New York.
Hibler, W. D. (1980), Modeling a variable thickness sea ice cover, *Mon. Weather Rev.*, *108*, 1943–1973.
Holloway, G., et al. (2007), Water properties and circulation in Arctic Ocean models, *J. Geophys. Res.*, *112*, C04S03, doi:10.1029/2006JC003642.
Hunke, E. C., and J. K. Dukowicz (1997), An elastic-viscous-plastic model for sea ice dynamics, *J. Phys. Oceanogr.*, *27*, 1849–1867.
Hunke, E. C., and J. K. Dukowicz (2002), The Elastic-Viscous-Plastic sea ice dynamics model in general orthogonal curvilinear coordinates on a sphere—Effect of metric terms, *Mon. Weather Rev.*, *130*, 1848–1865.
Hunke, E. C., and W. H. Lipscomb (2004), CICE: The Los Alamos Sea Ice Model, documentation and software, version 3.1, *Tech. Rep. LA-CC-98-16*, Los Alamos Natl. Lab., Los Alamos, N. M.
Jackett, D. R., and T. J. McDougall (1995), Minimal adjustment of hydrographic profiles to achieve static stability, *J. Atmos. Oceanic Technol.*, *12*, 381–389.
Jakobsson, M., N. Cherkis, J. Woodward, B. Coakley, and R. Macnab (2000), A new grid of Arctic bathymetry: A significant resource for scientists and mapmakers, *Eos Trans. AGU*, *81*, 89, 93, 96.
Kalnay, E., et al. (1996), The NCEP/NCAR 40-year reanalysis project, *Bull. Am. Meteorol. Soc.*, *77*, 437–471.
Kauffman, B. G., and W. G. Large (2002), The CCSM coupler, version 5.0.1, technical note, Natl. Cent. for Atmos. Res., Boulder, Colo. (Available at http://www.ccsm.ucar.edu/models/)
Kiehl, J. T., and P. R. Gent (2004), The Community Climate System Model, version two, *J. Clim.*, *17*, 3666–3682.
Köberle, C., and R. Gerdes (2003), Mechanisms determining the variability of Arctic sea ice conditions and export, *J. Clim.*, *16*, 2843–2858.
Large, W., and S. Yeager (2004), Diurnal to decadal global forcing for ocean and sea-ice models: The data sets and flux climatologies, *Tech. Note NCAR/TN-460 + STR*, CGD Div. Natl. Cent. for Atmos. Res., Boulder, Colo.
Large, W. G., G. Danabasoglu, S. C. Doney, and J. C. McWilliams (1997), Sensitivity to surface forcing and boundary layer mixing in a global ocean model: Annual-mean climatology, *J. Phys. Oceanogr.*, *27*, 2418–2447.
Lindsay, R. W. (1998), Temporal variability of the energy balance of thick Arctic pack ice, *J. Clim.*, *11*, 313–333.
Lipscomb, W. H. (2001), Remapping the thickness distribution in sea ice models, *J. Geophys. Res.*, *106*, 13,989–14,000.
Lipscomb, W. H., and E. C. Hunke (2004), Modeling sea ice transport using incremental remapping, *Mon. Weather Rev.*, *132*, 1341–1354.
Lythe, M. B., and D. G. Vaughan (2001), BEDMAP: A new ice thickness and subglacial topographic model of Antarctica, *J. Geophys. Res.*, *106*, 11,335–11,351.
Maykut, G. A. (1982), Large-scale heat exchange and ice production in the central Arctic, *J. Geophys. Res.*, *87*, 7971–7984.
Parkinson, C. L., and W. M. Washington (1979), A large-scale numerical model of sea ice, *J. Geophys. Res.*, *84*, 311–337.
Paulson, C. A., and J. J. Simpson (1977), Irradiance measurements in the upper ocean, *J. Phys. Oceanogr.*, *7*, 952–956.
Persson, P. O. G., C. W. Fairall, E. L. Andreas, P. S. Guest, and D. K. Perovich (2002), Measurements near the Atmospheric Surface Flux Group tower at SHEBA: Near-surface conditions and surface energy budget, *J. Geophys. Res.*, *107*(C10), 8045, doi:10.1029/2000JC000705.
Rigor, I., R. L. Colony, and S. Martin (2000), Variations in surface air temperature observations in the Arctic, 1979–97, *J. Clim.*, *13*, 896–914.
Rosati, A., and K. Miyakoda (1988), A general circulation model for upper ocean simulation, *J. Phys. Oceanogr.*, *18*, 1601–1626.
Röske, F. (2001), An atlas of surface fluxes based on the ECMWF reanalysis—A climatological data set to force global ocean general circulation models, *Tech. Rep. 323*, Max-Planck-Inst. für Meteorol., Hamburg, Germany.
Rossow, W. B., and R. A. Schiffer (1991), ISCCP cloud data products, *Bull. Am. Meteorol. Soc.*, *72*, 2–20.
Rothrock, D. A. (1975), The energetics of the plastic deformation of pack ice by ridging, *J. Geophys. Res.*, *80*, 4514–4519.
Serreze, M. C., and C. M. Hurst (2000), Representation of mean Arctic precipitation from NCEP-NCAR and ERA reanalyses, *J. Clim.*, *13*, 182–201.
Smith, R., and P. Gent (2002), Reference manual for the Parallel Ocean Program (POP), *Tech. Rep. LAUR-02-2484*, Los Alamos Natl. Lab., Los Alamos, N. M.
Smith, R. D., J. K. Dukowicz, and R. C. Malone (1992), Parallel ocean general circulation modeling, *Phys. D*, *60*, 38–61.
Smith, R. D., S. Kortas, and B. Meltz (1995), Curvilinear coordinates for global ocean models, *Tech. Rep. LA-UR-95-1146*, Los Alamos Natl. Lab., Los Alamos, N. M.
Smith, W. H., and D. T. Sandwell (1997), Global sea floor topography from satellite altimetry and ship depth soundings, *Science*, *277*, 1956–1962.
Thorndike, A. S., D. A. Rothrock, G. A. Maykut, and R. Colony (1975), The thickness distribution of sea ice, *J. Geophys. Res.*, *80*, 4501–4513.
Wu, B. Y., J. Wang, and J. Walsh (2004), Possible feedback of winter sea ice in the Greenland and Barents Sea on the local atmosphere, *Mon. Weather Rev.*, *132*, 1868–1876.
Xie, P., and P. A. Arkin (1996), Analyses of global monthly precipitation using gauge observations, satellite estimates, and numerical model predictions, *J. Clim.*, *9*, 840–858.
Zhang, J., and M. Steele (2007), The effect of vertical mixing on the Atlantic Water Layer circulation in the Arctic Ocean, *J. Geophys. Res.*, *112*, C04S04, doi:10.1029/2006JC003732.
Zhang, J., D. A. Rothrock, and M. Steele (1998), Warming of the Arctic Ocean by a strengthened Atlantic inflow: Model results, *Geophys. Res. Lett.*, *25*, 1745–1748.
Zillman, J. W. (1972), A study of some aspects of the radiation and heat budgets of the southern hemisphere oceans, *Meteorol. Stud. 26*, Bur. of Meteorol. Dep. of the Inter., Canberra, Australia.

M. M. Holland, National Center for Atmospheric Research, Boulder, CO 80307, USA.
E. C. Hunke, Climate, Ocean and Sea Ice Modeling Program, Los Alamos National Laboratory, MS-B216, Los Alamos, NM 87545, USA. (eclare@lanl.gov)